*31st EPS Conference on Plasma Phys. London, 28 June - 2 July 2004 ECA Vol.**28G**, P-5.164 (2004)*

JET ICRF antennas coupling on extreme plasma shapes

R. Bilato[1], M.-L. Mayoral[2], F. Rimini[3], M. Brambilla[1], D.A. Hartmann[1], A. Korotkov[2], P.U. Lamalle[4], I. Monakhov[2], J.-M. Noterdaeme[1,5], R. Sartori[6], and JET EFDA contributors[7]

[1] *MPI-IPP – Euratom Association – Boltzmannstr. 2, D-85748 Garching, Germany*
[2] *UKAEA – Euratom Association – Culham Science Center, Abingdon, OX14 3DB, UK*
[3] *CEA Cadarache – Euratom Association – Saint-Paul-Lez-Durance, France*
[4] *LPP-ERM/KMS – Euratom Association - TEC – Brussels, B-10000, Belgium*
[5] *Gent University, EESA Department – Gent, Belgium*
[6] *EFDA Close Support Unit, Boltzmannstr. 2, Garching, Germany*
[7] *See annex J. Pamela et al. 2003 19th IAEA Fusion Energy Conf. Conf. (Lyon, 2002)*

1 – Introduction. It is generally assumed that Ion Cyclotron Resonance Frequency (ICRF) antenna coupling is maximised when the shape of the plasma Last Closed Flux Surface (LCFS) matches the poloidal profile of the antenna. This is a relevant issue for plasmas at high triangularity, which are becoming more and more popular because of their favourable thermal confinement properties: in these configurations the LCFS is usually mismatched to the antenna curvature and the coupling could deteriorate, thereby limiting severely the ICRF power injection capability. While the dependence of the antenna coupling on the plasma-antenna distance in the equatorial plane of the tokamak is already well established [1] for the JET A2 antennas [2], the effect of lower and upper triangularity could not yet be adequately assessed. Dedicated experiments have now been performed on JET with four different plasma configurations (see fig. (1.a)), characterized by large range of variation of lower $\delta_{\rm lower}$ and upper $\delta_{\rm upper}$ triangularity.
In the frame of the transmission line theory, the antenna is described as a loading resistance $R_{\rm load}$ which terminates the transmission line of characteristic impedance Z_0 connecting the generator to the antenna. $R_{\rm load}$ is linked to the power transmitted by:

$$P_{\rm trans} = \frac{V_{\rm max}^2}{2\,Z_0}\,\frac{R_{\rm load}}{Z_0} \tag{1}$$

where $V_{\rm max}$ is the measured peak voltage in the coaxial. Taking into account the small losses in the transmission line and in the antenna $R_{\rm loss}$, the coupling resistance R_c is defined by $R_c = R_{\rm load} - R_{\rm loss}$. Since $V_{\rm max}$ cannot be higher than the maximum voltage sustainable in the line, R_c (or equivalently $R_{\rm load}$) represents the figure of merit of the performances of the ICRF system.
In the next section the experimental data are presented and discussed in terms of three relevant plasma-antenna distances, and a scaling of R_c with these distances is derived. The physics of the antenna coupling depends mainly on the propagation properties of the fast waves and on the linear and possible non-linear effects close to the antenna. Limiting the analysis to the role played by the evanescence layer close to the antenna, in section 3 we discuss a simple model which successfully reproduces the time evolution of the coupling resistance.

2 – Experimental setup and results. The set of dedicated discharges (from $\#58912$ to $\#58926$) are D(H) plasmas in L-mode with $I_p \approx 2\,\mathrm{MA}$, $B_0 \approx 2.7\,\mathrm{T}$, and $B(\mathrm{outer\ edge}) \approx 2\,\mathrm{T}$. For each configuration two slightly different plasma densities have been considered with the values on axis $n_e^{\rm axis} \approx 2$ and $2.5\ 10^{19}\,m^{-3}$. Only the frequency $\nu = 42\ \mathrm{MHz}$ and the dipole phasing ($[0, \pi, 0, \pi]$) have been examined; the rf power in antennas A and B was $1\,\mathrm{MW}$, and in antennas C and D only $\approx 0.2\,\mathrm{MW}$. According to these parameters the fundamental cyclotron resonance of the hydrogen is close to the plasma centre. The plasma configurations considered are the so-called **DOC_U**, **V/SFE/LT**, **HT3**, and **ITER-like**. Fig. (1.a) shows the poloidal plasma shape of the four configurations together with the poloidal location of the ICRF antennas. Also shown in fig. (1.a) are the

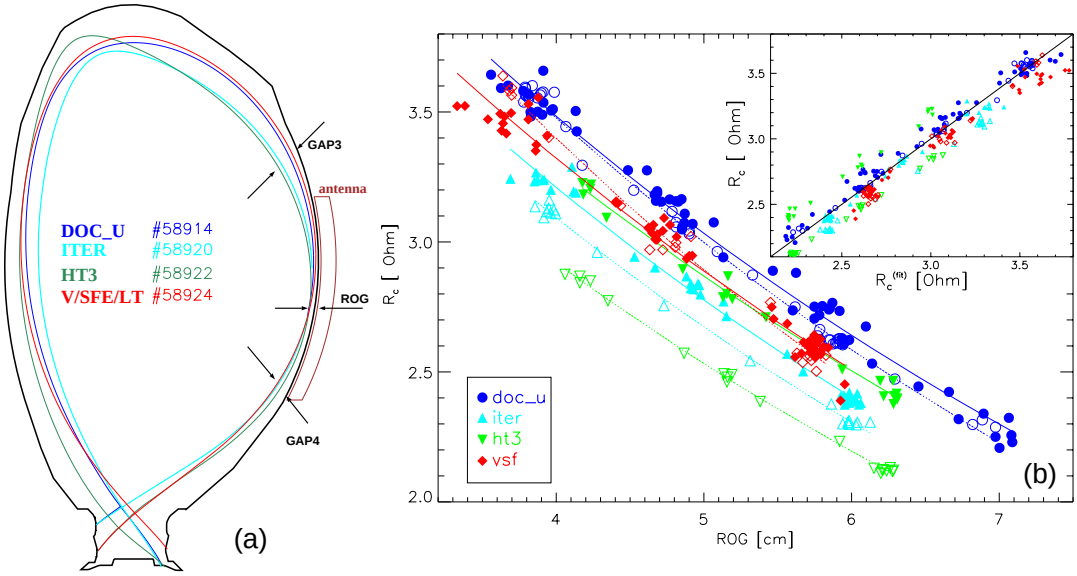

Figure 1: The poloidal plasma shapes of the here-considered configurations are reported in frame (a). The values of the here-relevant configuration parameters are reported in table (1). In frame (b) the values of R_c sampled in the time window $[15, 20]$ sec are plotted as function of ROG. The open and the filled symbols refer respectively to $n_e^{\rm axis} = 2. \cdot 10^{19}\,{\rm m}^{-3}$ and $n_e^{\rm axis} = 2.5 \cdot 10^{19}\,{\rm m}^{-3}$. In the inset R_c, sampled in $[13, 20]$ sec, is reported as function of $R_C^{\rm (fit)}$ (eqn. (2)).

poloidal positions close to the antennas at which the distance of the LCFS from the wall is evaluated by the magnetic reconstructing code EFIT, namely ROG, GAP3, and GAP4: the values of differences GAP3-ROG and GAP4-ROG are reported in table (1). The time trace of each discharge is characterized by two time windows: in the first $[13, 15]$ sec either GAP3 (for **HT3** and **ITER-like**) or GAP4 (for **DOC_U** and **V/SFE/LT**) is continously varied in order to achieve the final shape; in the second time window $[15, 20]$ sec, when the planned plasma shape is achieved, ROG is varied continously. In the following, we consider the coupling resistance of the antenna A averaged over the four straps and time-averaged over $100\,{\rm ms}$. Fig. (1.b) shows R_c sampled in $[15, 20]$ sec as function of ROG for the four different configurations and the two plasma densities. In all these discharges the R_c dependence on ROG is exponential, with almost the same e-folding length. However, the absolute value R_c depends appreciably on the plasma configuration, confirming that the best coupling is achieved with a plasma shape matching the antenna curvature (**DOC_U** and **V/SFE/LT**). Moreover, at high triangularity (**ITER-like** and **HT3**) R_c improves by increasing the plasma density.
By sampling R_c in the whole time interval $[13, 20]$ sec, one can have a rough estimate of the R_c dependences on GAP3 and GAP4. The experimental data are fitted by the following function:

$$R_c^{\rm (fit)} = R_0 \cdot \exp\Big\{ -14.87_{\rm m^{-1}} \cdot {\rm ROG} \; -0.75_{\rm m^{-1}} \cdot {\rm GAP3} \; + \; 1.01_{\rm m^{-1}} \cdot {\rm GAP4} \Big\} \qquad (2)$$

with $R_0 = 5.88\,\Omega$ and $\sigma \equiv [\langle (R_c - R_c^{\rm (fit)})^2 \rangle / \langle R_c^2 \rangle]^{1/2} = 0.037$. In the inset of fig. (1.b) the experimental values of R_c are plotted as function of the corresponding $R_c^{\rm (fit)}$ values. The fit (2) confirms that the plasma distance in the equatorial plane ROG is by far the most important parameter among the three. The peculiar dependence of R_c on GAP4, namely that R_c increases when GAP4 is increased, is not new for the A2 antennas, and this could be explained in terms of the connection of the magnetic field lines passing in front of the antenna with the plates of the divertor. Since the coefficients of the fit (2) are expected to depend on the plasma density, the confinement mode, the frequency, and the antenna phasing, the applicability of fit (2) is unavoidably limited to the range of parameters summarized at the beginning of this section.

Config. name	$\delta_{\rm lower}$	$\delta_{\rm upper}$	GAP3-ROG [cm]	GAP4-ROG [cm]
DOC_U	0.36	0.23	2	7
ITER-like	0.44	0.48	9	6
HT3	0.37	0.46	12	3
V/SFE/LT	0.21	0.23	2	6

Table 1: The values of the upper $\delta_{\rm upper}$ and lower $\delta_{\rm lower}$ triangularity, and the GAP3-ROG and GAP4-ROG values of the four plasma configurations of the set of the discharges under consideration.

3 – Modelling. The exponential dependence on the antenna-plasma distance of R_c in eqn. (2) is due to a non-negligible evanescence layer in front of the antenna, through which the waves must tunnel in order to propagate inside the plasma. In fact the fast waves in the ion cyclotron range of frequencies can propagate only when the plasma density is above the so-called cutoff density. In slab approximation with $x,\ y, \text{and}\ z$ pointing respectively in the radial, poloidal, and toroidal directions, the effects of this wave tunnelling on the transmitted power can be described in terms of the wave fields at the antenna $E_y^{\rm ant}$ as follows:

$$P_{\rm trans} \propto \sum_{n_z=-N_z}^{N_z} {\rm Im}\left\{ \left(E_y^{\rm ant}(n_z)\right)^* \, Y_{\rm pl} \, E_y^{\rm ant}(n_z) \right\} = P_0 \sum_{n_z=-N_z}^{N_z} J_{\rm ant}^2(n_z) \, e^{-k_0 \, \Gamma\left(\eta(n_z)\right)} \qquad (3)$$

where: $Y_{\rm pl}$ is the admittance of the evanescence layer and $\eta(n_z) = \int_0^{x_{\rm cutoff}(n_z)} |n_x(x,n_z)| \, {\rm d}x$ the optical thickness; $k_0 = \omega/c$ is the wavevector in vacuum, n_x and n_z are respectively the radial and toroidal components of the refractive index, and $x_{\rm cutoff}(n_z)$ is the width of the evanescence layer; $J_{\rm ant}^2(n_z)$ is the nominal spectrum of the currents obtained assuming that they are uniform along the toroidal direction and that the antenna elements are all equal and toroidally equispaced:

$$J_{\rm ant}(n_z) = \frac{\sin\left\{ N_{\rm g} \Big[k_0 \, (w+g) \, n_z - \Delta\phi \Big] / 2 \right\}}{N_{\rm g} \, \sin\left\{ \Big[k_0 \, (w+g) \, n_z - \Delta\phi \Big] / 2 \right\}} \, \frac{\sin(k_0 \, w \, n_z/2)}{k_0 \, w \, n_z/2} \qquad (4)$$

with: N_g is the number of elements of which the antenna is made; w and g are the width and the distance between the antenna elements; $\Delta\phi$ is the phase difference between two closest antenna elements. The exponent $\Gamma(\eta)$ in eqn. (3) accounts for the dependence of $P_{\rm trans}$ on the optical thickness η, and it can be estimated in two extreme cases: if the density is assumed homogeneous with a sharp discontinuity at the cutoff, then $\Gamma(\eta) \approx \eta$. If, on the other hand, a continuous linear density profile is assumed, $\Gamma(\eta) \approx 0.62\,\eta + 0.46\,\eta^2$ (for $0 \le \eta \le 3$). Empirically, for the discharges under consideration the best fit is with $\Gamma(\eta) \approx \eta$. The nominal power spectrum of the JET A2 antennas is shown in fig. (2.a) together with the cutoff density as function of the toroidal wavevector $k_\phi = k_0 \, n_z$. To evaluate $x_{\rm cutoff}(n_z)$ it is reasonable to use the cold plasma approximation, which requires only the knowledge of the confining magnetic field and the plasma density profile. The former is derived from the magnetic reconstruction, whereas the Lithium beam diagnostic has been used to monitor the density profile. Upon using eqn. (3) into eqn. (1), an equivalent expression for R_c can be derived. However, it is not possible to obtain the absolute value of R_c since P_0 is unknown. To estimate P_0 it is necessary to use complex numerical tools which take into account selfconsistently both the three-dimensional antenna geometry and the plasma dielectric properties. Instead, we have used eqn. (3) to study the relative changes of R_c during the evolution of the discharge. Relatively to a **DOC_U** discharge, the time traces of the experimental relative changes of R_c for each of the four straps are reported in fig. (2.b), together with the prediction based on eqn. (3) and (4). Since the four straps have different electrical and mechanical properties [2], the coupling resistance differs in magnitude (as reported in the legend) but has a similar time evolution. The goodness of the agreement between the

model and the experimental values, obtained also for the other discharges, confirms the importance of the density profile at the plasma edge in the ICRF antenna performances [1].

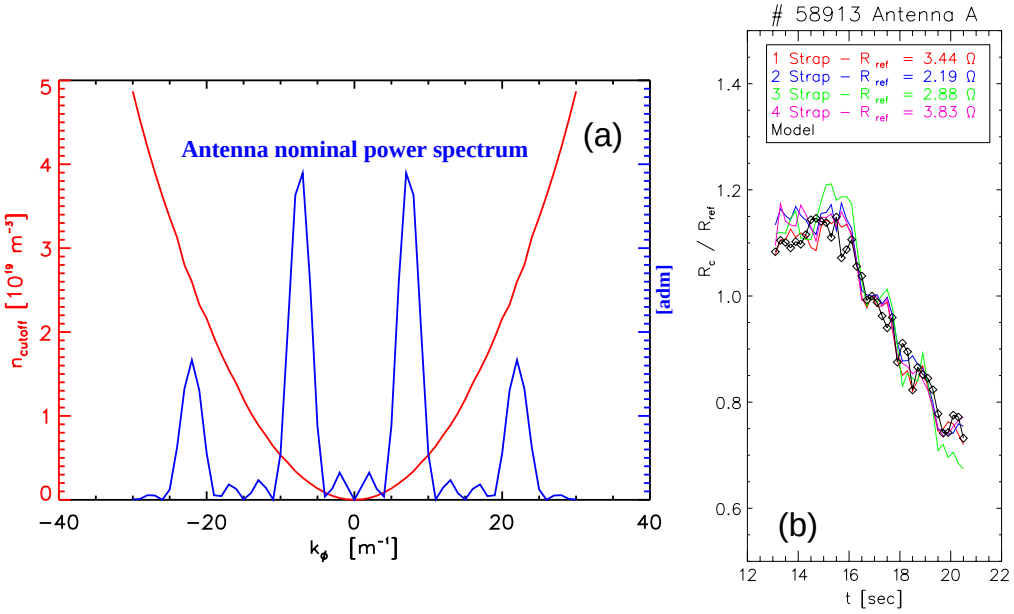

Figure 2: The frame (a) shows the cutoff density as function of the toroidal wavevector. In the same frame it is reported the normalized nominal power spectrum of the JET-A2 antennas with phasing $[0,\ \pi,\ 0\,\pi]$ and frequency $\nu = 42$ MHz. In frame (b) the time trace of the experimental values of the relative change of R_c (DOC_U discharge) of each of the four straps of antenna A is reported together with the prediction of the model based on eqn. (3) and (4).

4 – Conclusions. The fit (2) is based on the coupling resistance averaged over the four antenna straps and this is certainly a rough simplification of the reality, since the inner and the outer straps have rather different coupling properties [2]. None the less, in view of the ICRF system operation, it is reasonable to address the global behaviour of the antenna, and this analysis confirms that the plasma-antenna distance is by far the most important parameter for the coupling optimization [1]. Due to the exponential dependence on ROG, R_c can be substantially improved by reducing the evanescence layer in front of the antenna, namely by making the plasma as close as possible to the antenna. Unfortunately for ROG$< 3-4$ cm the ICRF coupling improvement is counterbalanced by a sharp increase of the power threshold for the L-H transition [3]. Thus, if the plasma-antenna distance cannot be reduced below $3-4$ cm, a favourable plasma shape (high $\delta_{\rm lower}$ and low $\delta_{\rm upper}$) can improve the antenna coupling, and this is more evident at lower plasma density (R_c is increased of about $20\,\%$ going from **HT3** to **DOC_U**, as shown in fig. (1.b)).
In the future this set of dedicated discharges characterized by a wide range of plasma shapes should be analyzed with antenna codes which deal with both the 3-dimensional antenna geometry and the plasma dielectric properties. We hope that this modelling will shed more light on the electrical behaviour of the ICRF A2 antenna when the edge plasma is varied.

Bibliography

[1] D.A. Hartmann *et al.*, "Coupling resistance of the JET ICRH A2 Antennas in the divertor configuration Mark II GB", Proc. $14^{\rm th}$ RF Topical Conference - AIP **595** (2001) 130.
[2] A. Kaye *et al.*, "Present and future JET ICRF antennae", Fus. Eng. Design **24** (1994) 1.
[3] The JET Team (presented by E. Righi), Proc. $18^{\rm th}$ Fusion energy Conference, Sorrento 2000, IAEA, Vienna, 2000, IAEA-Exp5-31.